Ultrafast and Long-Range Energy Transfer from Plasmon to Molecular Exciton

Fatimah Rudayni,[1,2] Tika R. Kafle,[1,3,*] Jack Waters,[1] Kushal Rijal,[1] Wai-Lun Chan[1,*]

1. Department of Physics and Astronomy, University of Kansas, Lawrence, KS 66045, United States

2. Department of Physics, Jazan University, Jazan 45142, Saudi Arabia

3. Department of Physics and JILA, University of Colorado, Boulder, CO 80309, United States

Abstract:

By using a model interface consisting of a metallic grating and zinc phthalocyanine (ZnPc) molecules, we temporally and spatially resolve the energy transfer process from plasmon to molecular exciton *via* the plasmon-induced resonance energy transfer (PIRET) mechanism. It is found that the energy transfer can occur within 30 fs for a distance of 20 nm. The energy transfer range is much larger than that of typical hot carrier transfer and molecule-to-molecule energy transfer processes. Hence, this ultrafast and long-range plasmon-induced energy transfer channel is especially useful for boosting the exciton/free carrier generation yield in semiconductor layers. Moreover, the enhancement in the exciton production yield does not diminish even when the photon energy is lowered towards the optical absorption edge of ZnPc. Therefore, the observed energy transfer process can extend the optical absorption to frequencies below the optical bandgap of the molecule.

* Corresponding authors:

tika.kafle@colorado.edu (T. R. Kafle); wlchan@ku.edu (W. L. Chan)

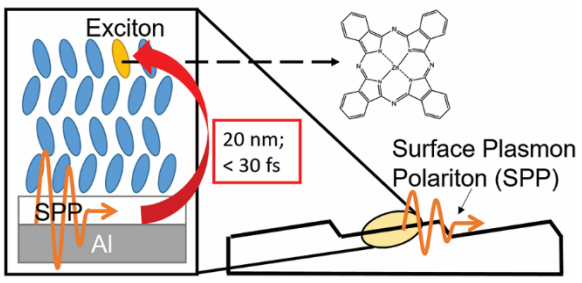

TOC figure

Introduction

In thin film optoelectronic devices, metallic nanoparticles are often used to increase the carrier/exciton generation in the photo-active layer through the excitation of surface plasmon at the surface of the nanoparticle. Surface plasmon can enhance the charge/exciton generation yield in a nearby semiconductor layer *via* several mechanisms. First, sub-wavelength nanoparticles are strong scatterers that can trap light into a very small volume, which significantly enhance the optical absorption in nearby semiconductor.[1-2] Indeed, this light trapping mechanism is commonly used to enhance the light absorption in thin film photovoltaics.[3-4] Second, charges can be harvested from surface plasmons through hot electron and hot hole transfers.[5-8] Plasmon relaxation generates hot electrons and holes in the metal, which can then inject into a nearby semiconductor to produce long-lived free electrons and holes. Third, if the semiconductor is excitonic in nature (e.g. organic materials, 2D materials, quantum dots), energy transfer can occur from the metal to the semiconductor *via* the coupling between the plasmon's collective dipole moment and the exciton's transition dipole moment.[9-14] If the plasmon-exciton coupling is strong enough, a hybrid state of plasmon and exciton can be formed, which allows ultrafast energy transfer between plasmons and excitons on an extremely short timescale (~ 10 fs) before the plasmon dephases.[15] Because the plasmon and hot carrier lifetimes are typically short (~ 10 – 100 fs),[16] the ultrafast plasmon-induced resonance energy transfer (PIRET) process provides a viable pathway for harvesting energies from the plasmon. More interestingly, the quantum mechanical PIRET process can produce excitons in the semiconductor even with the absorption of sub-bandgap photons.[10, 12] Harvesting sub-bandgap photons not only can broaden the spectral response, but it can also break the Shockley-Queisser limit in photovoltaics through a similar mechanism employed in intermediate-band solar cells.[17]

Despite of the interesting physics of the PIRET, its impact is often masked by other light enhancement mechanisms that produce similar outcomes. Hence, PIRET or, more generally, the energy transfer induced by the strong plasmon-exciton coupling is a rather elusive process.[9-10, 18] The extremely fast energy transfer process (~ 10 fs) also makes probing its dynamics challenging. Without unveiling the transfer dynamics, it is difficult to predict how different plasmon-induced energy and charge transfer pathways, and relaxation/dephasing processes would compete with each other. In this work, we use a model system that consists of a metallic grating and a commonly used organic semiconductors, zinc phthalocyanine (ZnPc), to study the energy transfer from surface plasmon polaritons (SPP) to exciton. Most works on energy transfer between plasmon and molecular exciton probe the plasmon-exciton coupling spectroscopically in the frequency domain.[13, 19-20] Here, we employ time-resolved two-photon photoemission spectroscopy (TR-TPPE) to measure the ultrafast energy transfer process from the SPP to molecular exciton in the time domain. The surface sensitive nature of the photoemission probe further allows us to determine the energy transfer distance in addition to the dynamics. We found that the SPP transfers its energy to ZnPc molecules in the first ~ 30 fs after photoexcitation for a distance of ~ 20 nm. The observed transfer range is much longer than that of typical hot-electron transfers (~ a few nm[7]), which can be attributed to the long decay length of the plasmonic field. By varying the photon energy from the peak to the edge of the ZnPc's absorption peak, we demonstrate that the exciton generation yield can be enhanced by a factor of ~ 3 - 4 throughout the spectral range, even at a photon energy ~ 0.2 eV lower than the ZnPc's optical bandgap. Hence, the process can be tuned to extend the spectral range for the absorption below the molecule's bandgap. The ultrafast, long-range PIRET makes it a desirable channel for energy harvesting.

Experimental Method

Sample preparation. A commercial reflective diffraction grating (Thorlabs, GR13-0605) with 600 lines/mm and Al as the metallic layer was used to generate the SPP. The grating was outgassed at 100 °C for 16 hours in an ultrahigh vacuum (UHV) chamber with a base pressure of 1×10^{-9} Torr. Then, ZnPc molecules (Luminescence Technology, >99%) was thermally evaporated onto the grating (with a size of 1 cm × 1 cm) in the UHV chamber at room temperature. The deposition rate was kept at 0.7 – 0.8 Å/min. The thickness of the ZnPc was monitored using a quartz crystal microbalance. After the ZnPc deposition, the sample was transferred to the photoemission chamber where the photoemission experiments were performed. The base pressure of the photoemission chamber is around 8×10^{-11} Torr.

TR-TPPE spectroscopy. TR-TPPE spectroscopy was used to measure the energy and population of excited electrons in the sample, which enables us to probe the energy transfer process. The sample was excited by 25-fs pump pulses with its central wavelength varied from 660 nm to 780 nm. For the photoemission probe, 65-fs probe pulses with a wavelength of 270 nm were used to ionize the excited electron. The kinetic energy of photoelectrons was measured using a hemispherical analyzer equipped with an imaging detector (Phoibos 100, SPECS). The pump and probe beams were generated by using the outputs of two noncollinear optical parametric amplifiers (Orpheus - 2H and Orpheus - 3H, Light Conversion), which were pumped by a Yb:KGW regenerative amplifier running at 125 kHz (Pharos - 10 W, Light Conversion). Both beams had a full-width half-maximum (fwhm) size of 0.8 mm at the sample. All experiments were done at room temperature. The pulse energy for the pump and probe pulses were 280 nJ and 10 nJ, respectively.

Results and Discussion

Typically, SPP cannot be excited on a flat metal surface because of constraints imposed by momentum and energy conservation. For photons and SPPs that have the same frequency *f*, the photon momentum projected onto the sample surface is always smaller than the SPP momentum.[21] Hence, the energy and momentum cannot be conserved simultaneously. To compensate for this "missing" momentum, a diffraction grating with a well-defined periodicity *L* can be employed.[21] The SPP with a wavevector k_{SPP} can then be excited when the following momentum conservation relationship is fulfilled:

$$k_{SPP}(f) = \frac{2\pi f}{c}\sin\theta + n\frac{2\pi}{L}, \qquad (1)$$

where *n* is any integers and θ is the incident angle of the light. The frequency dependent k_{SPP} can be determined analytically by using the dielectric constant of the metallic layer. In our case, the dielectric of Al reported in Ref. [[22]] is used. The first and second terms on the right-hand side represented the momentum contributed by the photon and the grating, respectively. Hence, for incident light with a particular *f*, the SPP can only be excited when θ satisfies Eq. 1.[21] We will refer this to as the resonant angle, and its value depends on *f*.

A commercial reflective diffraction grating (Thorlabs, GR13-0605) with 600 lines/mm and an Al metallic layer is used for the SPP excitation. The sample geometry is shown in Fig. 1a. To measure the energy transfer from SPPs to excitons, an ultrathin (~ 2 – 20 nm) ZnPc layer is deposited onto the grating. ZnPc is chosen because a strong coupling between SPP and exciton in similar pi-conjugated molecules has been previously observed.[13, 15, 19] In the TR-TPPE experiment, the sample is excited by 25 fs pump pulses with a tunable wavelength of 660 nm – 780 nm. We note that ZnPc aggregates have two optical absorption peaks located at ~600 nm and 680 nm (the two peaks are known as the Q-band).[23] Longer pump wavelengths enable us to study the plasmon-exciton energy transfer *via* the absorption of sub-bandgap photons. Because of the surface

sensitivity of the photoemission probe (for organic materials, probe depth ~ 1 – 3 nm at a kinetic energy ~ 5 eV above Fermi level.[24-25]), the signal is primarily originated from the exciton near the surface of the ZnPc layer,[26-27] and is insensitive to the hot electrons in the SPP that is located in the buried metal layer. As we will show, this can be further confirmed by the observation that similar spectra can be obtained with different ZnPc thicknesses (2 – 20 nm) and with ZnPc deposited on a flat SiO_2/Si substrate.

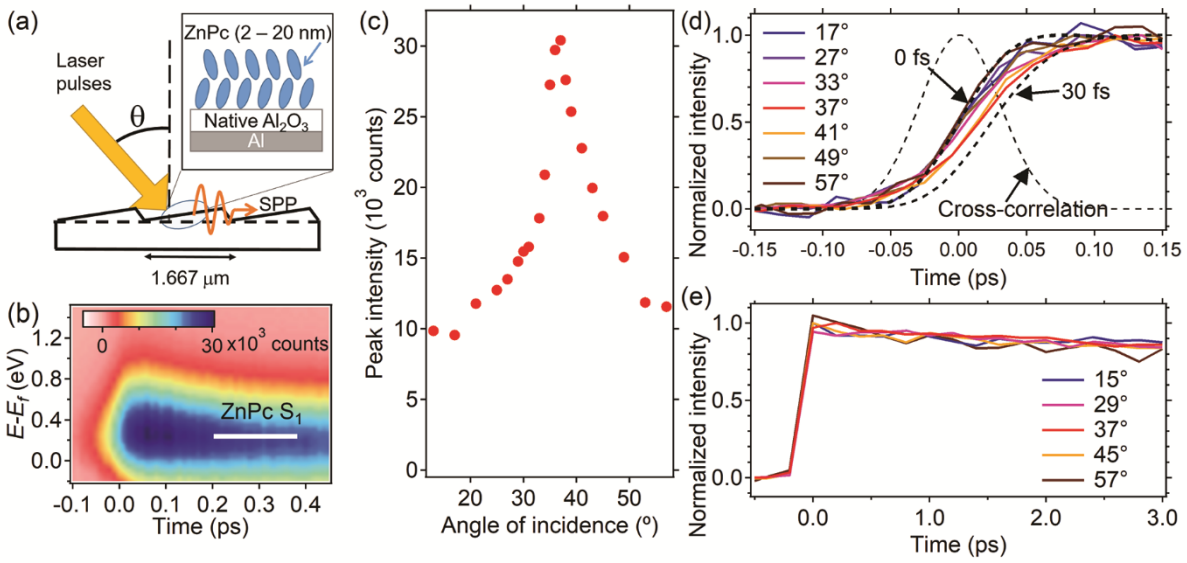

Figure 1: (a) A schematic shows the ZnPc/grating sample. The incident angle θ of the pump and probe beams is indicated on the figure. The SPP is generated in a direction parallel to the global surface (dashed line) of the grating. (b) A TR-TPPE spectrum of the 2-nm ZnPc/grating sample collected with a pump wavelength of 705 nm and θ = 37°. The peak is assigned to the ZnPc's S_1 exciton. (c) The peak intensity of the ZnPc's S_1 peak as a function of θ. (d, e) The temporal dynamics of the normalized TPPE intensity on two different timescales. Values of θ for different curves are shown in the figure legend. In (d), the simulated curves for 0 fs and 30 fs energy transfer times and the cross-correlation of the pump and probe pulses are shown as dashed lines.

Figure 1b shows a typical TR-TPPE spectrum obtained from a 2 nm-ZnPc/grating sample pumped at 705 nm. A band of excited states centered at an energy ~ 0.2 eV above the Fermi level E_f is observed. Very similar TR-TPPE spectra can be found in ZnPc films deposited on various substrates.[26-29] Following our previous works, we assigned this peak to the ZnPc's S_1 exciton. The S_1 population is not immediately quenched by the metal layer (Al) because the ZnPc is separated

from Al by the native oxide layer on the Al surface (Fig. 1a). We note that oxide growth on an Al surface is a self-limiting process and the thickness of the native oxide on Al is around 3 nm.[30] The S_1 state is rather long-lived, and its dynamics closely matches with our previous measurement of ZnPc's S_1 dynamics when ZnPc were deposited on a SiO_2 (native oxide)/Si surface (supporting information, Fig. S1). This confirms that we are probing the S_1 exciton generated in the ZnPc film.

A 705-nm (1.76 eV) photon can directly excite the ZnPc's S_1 and a spectral feature same as the one shown in Fig. 1b can be observed at all incident angles (with or without SPP excitation). However, the TPPE intensity is clearly enhanced near the resonant angle at which the SPP is resonantly excited. Figure 1c shows the maximum TPPE intensity near time zero as a function of θ, the intensity is increased by a factor of ~ 3 at $\theta = 37°$. The intensity enhancement can be attributed to the increase of the S_1 exciton population. We note that the observation cannot be explained by the plasmonic-enhancement of the photoemission probe process. The probe beam has a very different wavelength (270 nm) than that of the pump beam (705 nm). Hence, the 270-nm probe has a very different resonant angle. As we will show, the $\theta = 37°$ agrees well with SPP excitation at a wavelength of 705 nm.

The 3-folded increase in intensity at the resonant angle implies that around two-third of S_1 excitons is produced by the energy transfer from SPP to exciton. If the S_1 is excited indirectly *via* the SPP, the signal rise time would increase because of a finite energy transfer time (τ) between plasmon and exciton. Figure 1d shows the temporal rise of the normalized TPPE intensity for various θ. At off-resonant angles (e.g. 17° and 57°), the temporal rise of the signal matches well with the instrumental rise time originated from the widths of pump (25 fs) and probe (65 fs) pulses (the dashed line labeled as $\tau = 0$ fs). This indicates that excitons are created directly by the optical excitation. On the other hand, at the resonant angle (37°), the signal rise time is slightly longer (the

slope of the curve is less steep). The slower exciton's population rise can be explained by the energy transfer from the SPP to the exciton, i.e. the photon first excites the SPP and the exciton is excited *via* the SPP-exciton coupling.

We can model the temporal rise of the signal by assuming that the exciton is populated by the SPP with an energy transfer time constant of τ, and by accounting for the finite duration of the pump and probe pulses. A similar model has been used to model the signal rise time in Ref. [31]. In this model, the pump pulse excites SPP (its population is represented by n_{spp}). The plasmon-to-exciton energy transfer process, occurring with a time constant of τ, populates the ZnPc exciton. The population of the exciton (n_{ex}), and hence the signal intensity, is modeled by solving the following differential equations:

$$\frac{\partial n_{spp}}{\partial t} = cI_{pump}(t) - \frac{n_{spp}}{\tau}, \tag{2a}$$

$$\frac{\partial n_{ex}}{\partial t} = \frac{n_{spp}}{\tau} - \frac{n_{ex}}{\tau_d}. \tag{2b}$$

Here, the finite duration of the pump pulse (fwhm = 25 fs) is included in $I_{pump}(t)$, which represents the pump pulse intensity, and c is a constant. The time constant τ_d represents the initial decay time constant of the TPPE signal. The n_{ex} is further convoluted with the temporal width of the probe pulse (fwhm = 65 fs) to model the experimental signal.

The dashed line labelled as τ = 30 fs represents the signal rise with a transfer time of 30 fs. All the experimental curves are enveloped between the 0-fs and the 30-fs curves. Hence, τ should be 30 fs or less. If we assume that the delayed rise is purely originated from the energy transfer time, the SPP-exciton coupling strength is roughly given by ħ/τ, which is ~ 20 meV for a 30-fs transfer time. However, we note that τ would also represent the dephasing time of the coherent oscillation of the SPP. Until the SPP dephases, energy can transfer continually from the SPP to

excitons.[10] Once the coherent oscillation dephases, the SPP can no longer transfer its energy to molecules and the exciton population ceases to increase. Hence, the measured τ can represent the SPP dephasing time with an actual energy transfer time being less than 30 fs. Nevertheless, both interpretations agree with an energy transfer time of 30 fs or less (or a coupling strength of 20 meV or larger).

After the initial excitation, the S_1 exciton has the same dynamics that is independent of the incident angle (Fig. 1e). We have also measured the S_1 exciton dynamics for delay times up to 300 ps, which is shown in Fig. 2. Two incident angles (35°, 55°) were chosen. According to Fig. 1c, SPP is resonantly excited at 35°, but not at 55°. The decay dynamics is essentially the same. The result shows that the same kind of S_1 exciton is created after the initial excitation, and the nature of the exciton does not depend on the excitation pathway, i.e. the lifetime is the same whether it is directly excited by a photon (55°) or indirectly *via* the SPP (35°).

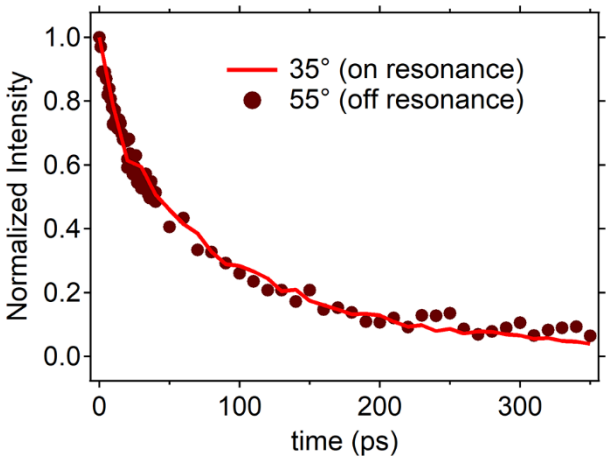

Figure 2: Normalized TPPE intensity for a 2-nm ZnPc film deposited on the Al grating. The intensity represents the ZnPc's S_1 population. A pump wavelength centered at 705 nm was used. The incident angle 35° and 55° corresponds to on and off resonance conditions for SPP excitation, respectively.

Compared to typical charge transfer processes, the plasmon-exciton energy transfer should have a much longer transfer range that is limited by the decay length of the plasmonic field instead

of the spatial extends of the electronic wavefunction. We can study this transfer range by increasing the ZnPc layer thickness. Because TPPE measures the exciton population near the ZnPc's surface, it probes the energy transfer from the buried metallic grating to the surface of the ZnPc layer. Hence, the transport distance being probed is roughly equal to the film thickness plus the thickness of the native oxide on the Al surface (~ 3 nm). Figure 3a shows the TPPE intensity as a function of the incident angle for film thicknesses up to 20 nm. For comparison, all curves are normalized by the measured intensity at off-resonant angles. Similar resonant behaviors can be observed at all thicknesses. Although the amount of intensity enhancement at the resonant angle generally decreases with an increasing film thickness, clear enhancement can still be observed even for a film thickness of 20 nm. We note that we have not conducted measurements beyond 20 nm, but the maximum energy transfer length can be larger than that. Two ways can limit the energy transfer distance. First, the incident light field can be absorbed by the ZnPc layer before it reaches the metal grating to excite the SPP. Using the dielectric constant for ZnPc that we measured in a previous work,[32] we found that $1/\alpha \sim 86$ nm at $\lambda \sim 700$ nm, where α is the absorption coefficient. Second, by using dielectric constants of ZnPc and Al, and equations in Ref. [[21]], we found that the SSP field has a decay length of ~ 210 nm at $\lambda \sim 700$ nm. Because the plasmon-exciton coupling strengthen is proportional to the square of the plasmonic field,[11] the coupling strength decreases with a decay length of ~ 105 nm. Accounting for the attenuations of both the incident field and the SPP field, we can estimate a composite decay length L with $1/L = 1/105 + 1/86$, which gives $L \sim$ 47 nm. Hence, the maximum transfer distance in our samples can be as large as ~ 50 nm. Finally, we note that the optical absorption from ZnPc limits the ultimate energy transfer distance in the current sample configuration. Alternatively, we would separate the grating and a thin ZnPc layer with a much thicker oxide layer and study the plasmonic enhancement as a function of the oxide

thickness. Because the oxide is transparent to the incident light, the transfer distance determined by this sample configuration will only be limited by the decay length of the plasmonic field. We would then establish the long-range nature of this energy transfer channel.

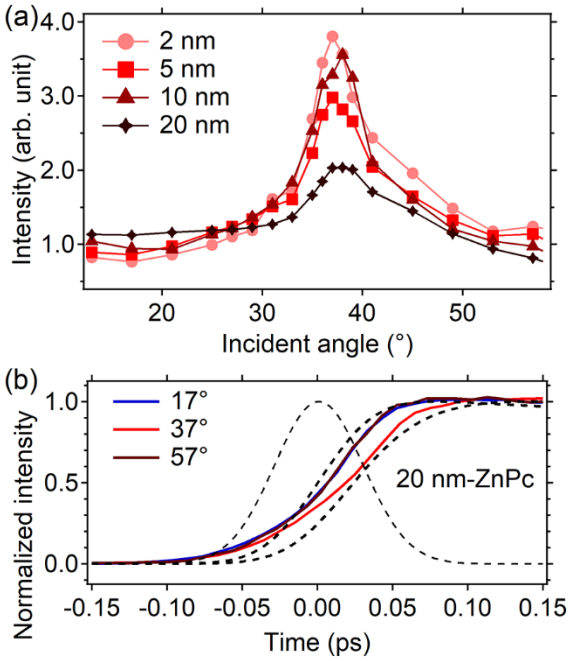

Figure 3: (a) The ZnPc S_1 peak intensity as a function of θ for samples with different ZnPc's thicknesses (indicated in the legend). The pump wavelength is 705 nm. (b) The temporal rise of the signal at the resonance (θ = 37°) and off the resonance (θ = 17°, 57°).

For the 20-nm sample, we have also measured the signal rise time for on (37°) and off (17°, 57°) resonant conditions. These data are shown in Fig. 3b. The temporal dynamics is similar to those observed for the 2-nm sample (Fig. 1d), which shows that the signal rise is delayed at the resonant angle. The data shows that the energy transfer can occur within 30 fs for a distance of 20 nm. The long energy transfer range further confirms that the exciton in ZnPc is populated by plasmon-exciton energy transfer rather than hot-carrier transfer. Hot electron and hole transfers from the metal to the molecule relies on the wavefunction overlapping and can only occur with molecules that are very close to the metal layer. Even accounting for exciton delocalization (in

ZnPc, we found an exciton delocalization size of ~ 4 nm[27]), hot charge transfer cannot produce excitons at the surface of a 20-nm ZnPc film within 30 fs.

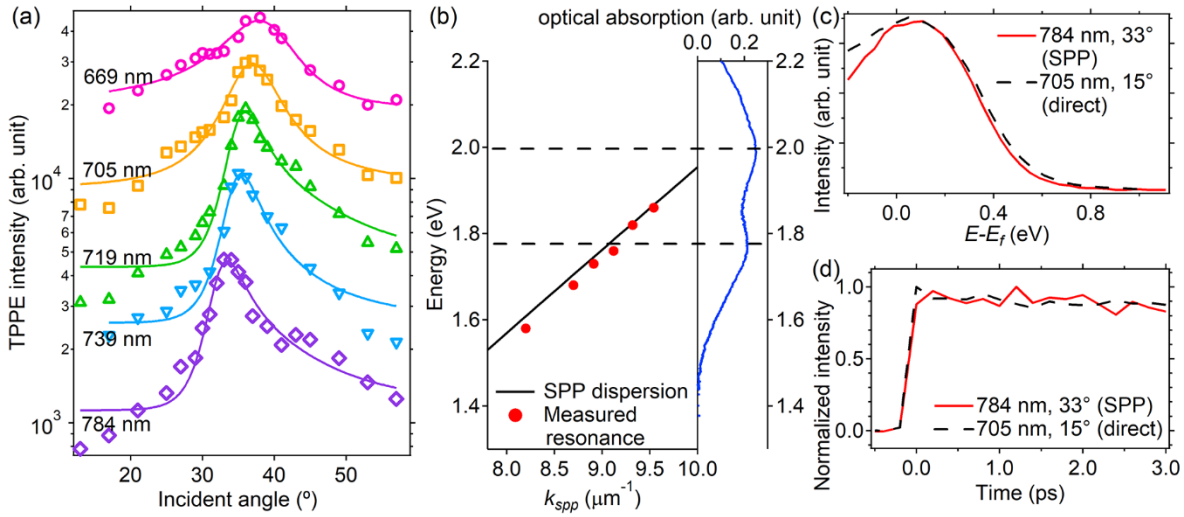

Figure 4: (a) The resonant curves collected at different pump wavelengths. The resonant angle shifts because of the SPP dispersion. (b) The experimentally measured SPP dispersion (solid circle) and the calculated SPP dispersion (solid line). For comparison, the optical absorption spectrum of a ZnPc film is shown on the right. The two horizontal lines represent the peak positions in the ZnPc's absorption spectrum. (c) The TPPE spectrum at two different experimental conditions in which excitons are populated indirectly by SPPs and directly by photons. (d) The temporal dynamics of the TPPE signal for the two conditions.

So far, the SPP is excited by pump pulses with a central wavelength of 705 nm. We also measured the dependence on the pump photon energy for the 2-nm sample. Figure 4a shows resonant curves collected at different pump wavelengths. The wavelengths indicated on the figure represent centroids of the fs-broadband pump pulses. The resonant angle clearly changes with the pump photon energy. The lineshape is asymmetric and it can be fit reasonably well with an asymmetric Lorentzian function.[33] The fit is used to determine the resonant angle. Using measured resonant angles and Eq. (1), we can determine the SPP's wavevector (k_{SPP}) for different photon energies (E). The E-k_{SPP} relationship is plotted in Fig. 4b. The experimentally determined data is shown as solid circles. Moreover, the SPP dispersion relationship can be determined analytically by using:[21]

$$k_{SPP} = \frac{\omega}{c}\sqrt{\frac{\varepsilon_i \varepsilon_m}{\varepsilon_i + \varepsilon_m}} \quad (3)$$

, where ω/c is the wavevector of the light, ε_i and ε_m are the dielectric constants for the incident medium and the metal, respectively. In our case, the incident medium is vacuum. We neglect the effect of the 2-nm ZnPc layer on the SPP dispersion because its optical thickness is much smaller than the photon wavelength. The dielectric constant of Al reported in Ref. [22] is used. The calculated dispersion is shown as the black solid line in Fig. 4b, which agrees well with the experimental measurement.

Typically, a strong plasmon-exciton coupling leads to an energy splitting at the crossing of the plasmon and exciton dispersion curves (usually referred to as avoided crossing).[19] In Fig. 4b, the experimental data points (solid circles) do not show a clear avoided crossing. The absence of an avoided crossing can be explained by the following reasons. First, the ZnPc crystal has a rather broad absorption peak because of the large intermolecular electronic coupling between molecules (~100 meV).[23] For reference, the absorption spectrum for a ZnPc film is shown on the right-hand side of Fig. 4b. Locations of the two absorption peaks are indicated by two dashed-horizontal lines. The width of each absorption peak is on the order of 100 meV, which is larger than the SPP-exciton coupling strengthen estimated from the time-resolved measurement (20 meV). Because the SPP would couple to singlet states that have different configurations within the broad absorption band,[23] and each of these configurations have slightly different energies, it is unlikely that the dispersion would show a clear, single avoided crossing. Second, the 25-fs pump laser pulse that we used have a large bandwidth (~100 - 200 meV – see Fig. S2 in the supporting information for the spectra). This will result in an "averaging" effect that basically lowers the energy resolution of our measurement.

Interestingly, the SPP can still enhance the exciton production yield effectively even when the pump photon energy is lower than the exciton energy. The lower energy peak in the ZnPc's absorption spectrum is centered at a wavelength of 700 nm. When the sample is pumped at 784 nm (at the edge of the absorption peak), the TPPE intensity, and hence the exciton population, can still be enhanced near the SPP resonant angle. Indeed, an enhancement factor of ~ 4.5 is found, which is even larger than the enhancement factor (~ 3) observed at 705 nm. This finding is interesting because the SPP-exciton coupling should be weaker when the spectral overlap between the SPP's and the exciton's absorption becomes smaller.[34] To understand this observation, we note that our enhancement factor is defined as the ratio of the exciton population when the SPP is resonantly excited and the exciton population when the SPP is not excited. Excitons can be created by both direct optical absorption and PIRET in the former case, while excitons can only be created by direct optical absorption in the latter case. To a first approximation, because the SPP-exciton coupling strength is proportional to the absorption cross section of ZnPc at the SPP frequency,[11] the exciton population produced by PIRET should decrease with a decrease in the ZnPc absorption. The exciton population produced by direct excitation is proportional to the ZnPc absorption as well. Hence, the enhancement factor should be insensitive to wavelength. However, the enhancement factor at 784 nm is larger than that at 705 nm. We do not have a simple explanation to this observation. However, it would be explained by the interference effect when two coupled states (plasmon and exciton in this case) are populated simultaneously by the laser pulse. As shown in a previous work,[35] when the energy detuning between the two coupled states is on the order of the coupling strength between the two states, the population of one of the states can be enhanced in the expense of the other. Therefore, the SPP-exciton coupling would enhance the direct optical excitation of ZnPc's exciton *via* such intensity borrowing mechanism. Because this mechanism

diminishes when the two states have the same energy,[35] it would be activated at 784 nm, but not at 705 nm, which would explain the larger enhancement factor at 784 nm.

As shown in Fig. 4c, the TPPE spectrum for S_1 excitons produced by the 784 nm excitation at the resonant angle has a same spectral shape as the spectrum produced by the 705 nm excitation at an off resonant angle. Moreover, S_1 excitons produced in both cases have the same dynamics (Fig. 4d). Hence, the S_1 exciton that is produced by direct optical excitation (705 nm, 15°) is essentially indistinguishable from the exciton produced by the SPP-exciton energy transfer (784 nm, 33°). Therefore, if the sample is set at an incident angle that can resonantly excites SPP at a sub-bandgap photon energy, not only that we can absorb more photons, but the same exciton can also be produced by a photon that has a lesser energy. This essentially extends the optical absorption beyond the absorption edge.

To compare the exciton-generation yield at different wavelengths, we normalize the TPPE intensity in Fig. 4a with the number of incident pump photons. The normalized TPPE counts, which is proportional to the exciton generation yield, is plotted as a function of the pump wavelength (Fig. 5). Data collected at four different incident angles are shown. Compared to the off-resonant angle (23°), the exciton-generation yield near the absorption edge is preferentially enhanced (red arrow) at $\theta \sim 32.5°$ and 35° when the SPP is resonantly excited at sub bandgap energies. Because the SPP energy depends on the incident angle, the population can be enhanced at a selected wavelength by varying θ. For example, at $\theta \sim 35°$ (green curve), the normalized count is slightly larger at ~720 - 740 nm than that at 700 nm because the SPP resonant angle at 740 nm is ~35°. Hence, the normalized intensity near 740 nm is selectively enhanced at $\theta = 35°$. Similar PIRET-induced sub-bandgap light absorption has been reported with Au/Cu_2O core/shell

nanoparticles.[12] Our results demonstrated that this interesting phenomenon can occur in solid-state organic thin films as well.

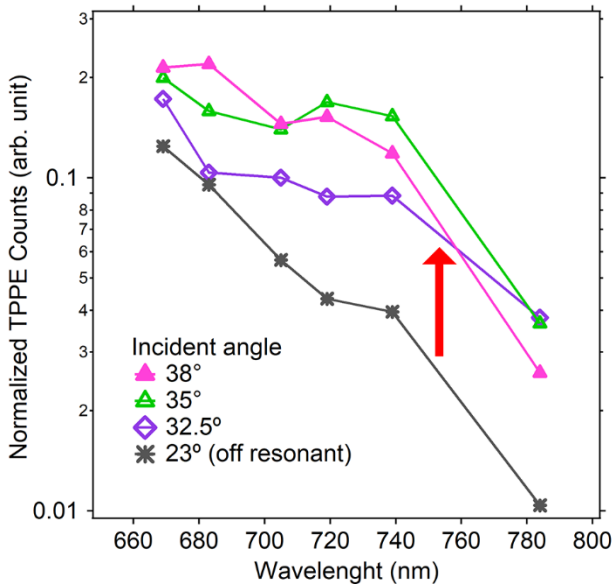

Figure 5: The TPPE signal normalized by the number of incident photons in the pump pulse is plotted as a function of the pump wavelength. The data at four different incident angles are shown. The normalized signal is proportional to exciton generation yield. The SPP-exciton energy transfer can preferentially enhance the exciton production in the sub-bandgap region (red arrow).

Conclusion

By using a model organic semiconductor/metal grating interface, we demonstrate that effective energy transfer can exist between plasmon and exciton. The plasmon-to-exciton energy transfer time is fast enough (< 30 fs) to allow significant energy transfer from plasmon to exciton despite of the very short dephasing time of the SPP. Moreover, the transfer range is large (~ 20 nm) as compared to that of typical charge and exciton transfer processes. For the ZnPc/Al grating system, the plasmon-to-exciton energy transfer increases the exciton-generation yield in ZnPc by a factor of ~3 – 4. The enhancement remains pronounced even when the photon energy is lower than the energy of the ZnPc's optical absorption peak. Hence, the plasmon-to-exciton energy transfer can essentially change the spectral sharp of the optical absorption peak and extend the

optical absorption beyond the optical bandgap. This ultrafast and long-range energy transfer channel can be useful for harvesting solar energy especially in ultrathin photovoltaics and optoelectronic devices in which the optical absorption from the optically thin semiconductor layer is limited.

Supporting Information

Additional data on ZnPc's S_1 exciton dynamics and the spectra of the pump laser.

Acknowledgement

This work was supported by US National Science Foundation grants DMR-1351716, and DMR-2109979. The support by the University of Kansas General Research Fund allocation #2151080 is also acknowledged. F.R. acknowledges the scholarship support from Jazan University.

References:

1. Schuller, J. A.; Barnard, E. S.; Cai, W. S.; Jun, Y. C.; White, J. S.; Brongersma, M. L., Plasmonics for Extreme Light Concentration and Manipulation. *Nat. Mater.* **2010**, *9*, 193-204.
2. Aydin, K.; Ferry, V. E.; Briggs, R. M.; Atwater, H. A., Broadband Polarization-Independent Resonant Light Absorption Using Ultrathin Plasmonic Super Absorbers. *Nat. Commun.* **2011**, *2*, 517.
3. Pala, R. A.; Liu, J. S. Q.; Barnard, E. S.; Askarov, D.; Garnett, E. C.; Fan, S. H.; Brongersma, M. L., Optimization of Non-Periodic Plasmonic Light-Trapping Layers for Thin-Film Solar Cells. *Nat. Commun.* **2013**, *4*, 2095.
4. Ferry, V. E.; Verschuuren, M. A.; Li, H. B. T.; Verhagen, E.; Walters, R. J.; Schropp, R. E. I.; Atwater, H. A.; Polman, A., Light Trapping in Ultrathin Plasmonic Solar Cells. *Opt. Express* **2010**, *18*, A237-A245.
5. Kim, M.; Lin, M.; Son, J.; Xu, H. X.; Nam, J. M., Hot-Electron-Mediated Photochemical Reactions: Principles, Recent Advances, and Challenges. *Adv. Opt. Mater.* **2017**, *5*, 1700004.
6. Wu, K.; Chen, J.; McBride, J. R.; Lian, T., Efficient Hot-Electron Transfer by a Plasmon-Induced Interfacial Charge-Transfer Transition. *Science* **2015**, *349*, 632-635.
7. Xu, C.; Yong, H. W.; He, J. L.; Long, R.; Cadore, A. R.; Paradisanos, I.; Ott, A. K.; Soavi, G.; Tongay, S.; Cerullo, G., et al., Weak Distance Dependence of Hot-Electron-Transfer Rates at the Interface between Monolayer Mos2 and Gold. *ACS Nano* **2021**, *15*, 819-828.
8. Tan, S. J.; Argondizzo, A.; Ren, J. D.; Liu, L. M.; Zhao, J.; Petek, H., Plasmonic Coupling at a Metal/Semiconductor Interface. *Nat. Photon.* **2017**, *11*, 806-812.
9. Wang, H.; Wang, H. Y.; Sun, H. B.; Cerea, A.; Toma, A.; De Angelis, F.; Jin, X.; Razzari, L.; Cojoc, D.; Catone, D., et al., Dynamics of Strongly Coupled Hybrid States by Transient Absorption Spectroscopy. *Adv. Funct. Mater.* **2018**, *28*, 1801761.
10. Cushing, S. K.; Wu, N. Q., Progress and Perspectives of Plasmon-Enhanced Solar Energy Conversion. *J. Phys. Chem. Lett.* **2016**, *7*, 666-675.

11. Hsu, L. Y.; Ding, W. D.; Schatz, G. C., Plasmon-Coupled Resonance Energy Transfer. *J. Phys. Chem. Lett.* **2017**, *8*, 2357-2367.
12. Li, J. T.; Cushing, S. K.; Meng, F. K.; Senty, T. R.; Bristow, A. D.; Wu, N. Q., Plasmon-Induced Resonance Energy Transfer for Solar Energy Conversion. *Nat. Photon.* **2015**, *9*, 601-607.
13. Collins, S. S. E.; Searles, E. K.; Tauzin, L. J.; Lou, M. H.; Bursi, L.; Liu, Y. W.; Song, J.; Flatebo, C.; Baiyasi, R.; Cai, Y. Y., et al., Plasmon Energy Transfer in Hybrid Nanoantennas. *ACS Nano* **2021**, *15*, 9522-9530.
14. Li, G. L.; Cherqui, C.; Bigelow, N. W.; Duscher, G.; Straney, P. J.; Millstone, J. E.; Masiello, D. J.; Camden, J. P., Spatially Mapping Energy Transfer from Single Plasmonic Particles to Semiconductor Substrates Via Stem/Eels. *Nano Lett.* **2015**, *15*, 3465-3471.
15. Vasa, P.; Wang, W.; Pomraenke, R.; Lammers, M.; Maiuri, M.; Manzoni, C.; Cerullo, G.; Lienau, C., Real-Time Observation of Ultrafast Rabi Oscillations between Excitons and Plasmons in Metal Nanostructures with J-Aggregates. *Nat. Photon.* **2013**, *7*, 128-132.
16. Gieseking, R. L. M., Plasmons: Untangling the Classical, Experimental, and Quantum Mechanical Definitions. *Materials Horizons* **2022**, *9*, 25-42.
17. Luque, A.; Marti, A.; Stanley, C., Understanding Intermediate-Band Solar Cells. *Nat. Photon.* **2012**, *6*, 146-152.
18. Li, T. E.; Cui, B. Y.; Subotnik, J. E.; Nitzan, A., Molecular Polaritonics: Chemical Dynamics under Strong Light-Matter Coupling. *Annu. Rev. Phys. Chem.* **2022**, *73*, 43-71.
19. Bigeon, J.; Le Liepvre, S.; Vassant, S.; Belabas, N.; Bardou, N.; Minot, C.; Yacomotti, A.; Levenson, A.; Charra, F.; Barbay, S., Strong Coupling between Self-Assembled Molecules and Surface Plasmon Polaritons. *J. Phys. Chem. Lett.* **2017**, *8*, 5626-5632.
20. Beane, G.; Brown, B. S.; Johns, P.; Devkota, T.; Hartland, G. V., Strong Exciton-Plasmon Coupling in Silver Nanowire Nanocavities. *J. Phys. Chem. Lett.* **2018**, *9*, 1676-1681.
21. Zayats, A. V.; Smolyaninov, I. I.; Maradudin, A. A., Nano-Optics of Surface Plasmon Polaritons. *Phys Rep* **2005**, *408*, 131-314.
22. McPeak, K. M.; Jayanti, S. V.; Kress, S. J. P.; Meyer, S.; Iotti, S.; Rossinelli, A.; Norris, D. J., Plasmonic Films Can Easily Be Better: Rules and Recipes. *Acs Photonics* **2015**, *2*, 326-333.
23. Feng, S. S.; Wang, Y. C.; Ke, Y. L.; Liang, W. Z.; Zhao, Y., Effect of Charge-Transfer States on the Vibrationally Resolved Absorption Spectra and Exciton Dynamics in ZnPc Aggregates: Simulations from a Non-Makovian Stochastic Schrodinger Equation. *J. Chem. Phys.* **2020**, *153*, 034116.
24. Seah, M. P.; Dench, W. A., Quantitative Electron Spectroscopy of Surfaces: A Standard Data Base For Electron Inelastic Mean Free Paths in Solids. *Surf. Interface Anal.* **1979**, *1*, 2-11.
25. Ozawa, Y.; Nakayama, Y.; Machida, S.; Kinjo, H.; Ishii, H., Maximum Probing Depth of Low-Energy Photoelectrons in an Amorphous Organic Semiconductor Film. *J. Electron. Spectrosc. Relat. Phenom.* **2014**, *197*, 17-21.
26. Wang, T.; Kafle, T. R.; Kattel, B.; Chan, W.-L., A Multidimensional View of Charge Transfer Excitons at Organic Donor–Acceptor Interfaces. *J. Am. Chem. Soc.* **2017**, *139*, 4098-4106.
27. Wang, T.; Chan, W. L., Dynamical Localization Limiting the Coherent Transport Range of Excitons in Organic Crystals. *J. Phys. Chem. Lett.* **2014**, *5*, 1812-1818.

28. Wang, T.; Liu, Q. F.; Caraiani, C.; Zhang, Y. P.; Wu, J.; Chan, W. L., Effect of Interlayer Coupling on Ultrafast Charge Transfer from Semiconducting Molecules to Mono- and Bilayer Graphene. *Phys. Rev. Appl.* **2015**, *4*, 014016.
29. Wanigasekara, S.; Rijal, K.; Rudayni, F.; Panth, M.; Shultz, A.; Wu, J. Z.; Chan, W. L., Using an Atomically Thin Layer of Hexagonal Boron Nitride to Separate Bound Charge-Transfer Excitons at Organic Interfaces. *Phys. Rev. Appl.* **2022**, *18*, 014042.
30. Evertsson, J.; Bertram, F.; Zhang, F.; Rullik, L.; Merte, L. R.; Shipilin, M.; Soldemo, M.; Ahmadi, S.; Vinogradov, N.; Carla, F., et al., The Thickness of Native Oxides on Aluminum Alloys and Single Crystals. *Appl. Surf. Sci.* **2015**, *349*, 826-832.
31. Rijal, K.; Rudayni, F.; Kafle, T. R.; Chan, W.-L., Collective Effects of Band Offset and Wave Function Dimensionality on Impeding Electron Transfer from 2D to Organic Crystals. *J. Phys. Chem. Lett.* **2020**, *11*, 7495-7501.
32. Kattel, B.; Qin, L.; Kafle, T. R.; Chan, W. L., Graphene Field-Effect Transistor as a High-Throughput Platform to Probe Charge Separation at Donor-Acceptor Interfaces. *J. Phys. Chem. Lett.* **2018**, *9*, 1633-1641.
33. Stancik, A. L.; Brauns, E. B., A Simple Asymmetric Lineshape for Fitting Infrared Absorption Spectra. *Vib. Spectrosc* **2008**, *47*, 66-69.
34. Cushing, S. K.; Li, J. T.; Bright, J.; Yost, B. T.; Zheng, P.; Bristow, A. D.; Wu, N. Q., Controlling Plasmon-Induced Resonance Energy Transfer and Hot Electron Injection Processes in Metal@TiO2 Core-Shell Nanoparticles. *J. Phys. Chem. C* **2015**, *119*, 16239-16244.
35. Chan, W. L.; Tritsch, J.; Dolocan, A.; Ligges, M.; Miaja-Avila, L.; Zhu, X. Y., Communication: Momentum-Resolved Quantum Interference in Optically Excited Surface States. *J. Chem. Phys.* **2011**, *135*, 031101.

Supporting Information

Ultrafast and Long-Range Energy Transfer from Plasmon to Molecular Exciton

Fatimah Rudayni,[1,2] Tika R. Kafle,[1,3,*] Jack Waters,[1] Kushal Rijal,[1] Wai-Lun Chan[1,*]

1. Department of Physics and Astronomy, University of Kansas, Lawrence, KS 66045, United States

2. Department of Physics, Jazan University, Jazan 45142, Saudi Arabia

3. Department of Physics and JILA, University of Colorado, Boulder, CO 80309, United States

[*] Corresponding authors:

tika.kafle@colorado.edu (T. R. Kafle);

wlchan@ku.edu (W. L. Chan)

A. Additional time-resolved two-photon photoemission spectroscopy (TR-TPPE) data

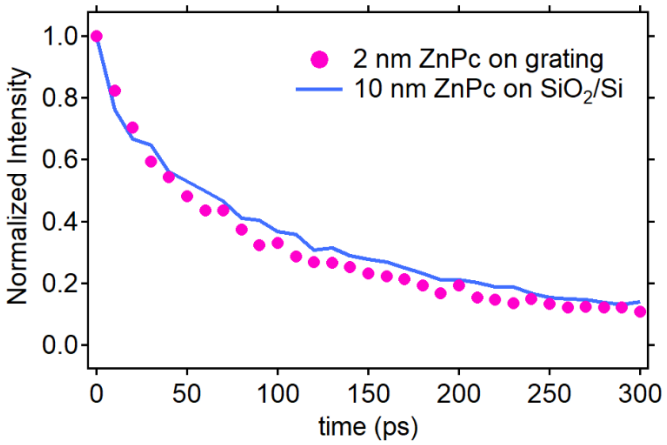

Figure S1: Temporal evolution of the ZnPc's S_1 population measured by TR-TPPE. For both measurements, the incident angle of the laser pulses was 30°.

B. Spectra for the pump laser pulses used in the TR-TPPE experiment

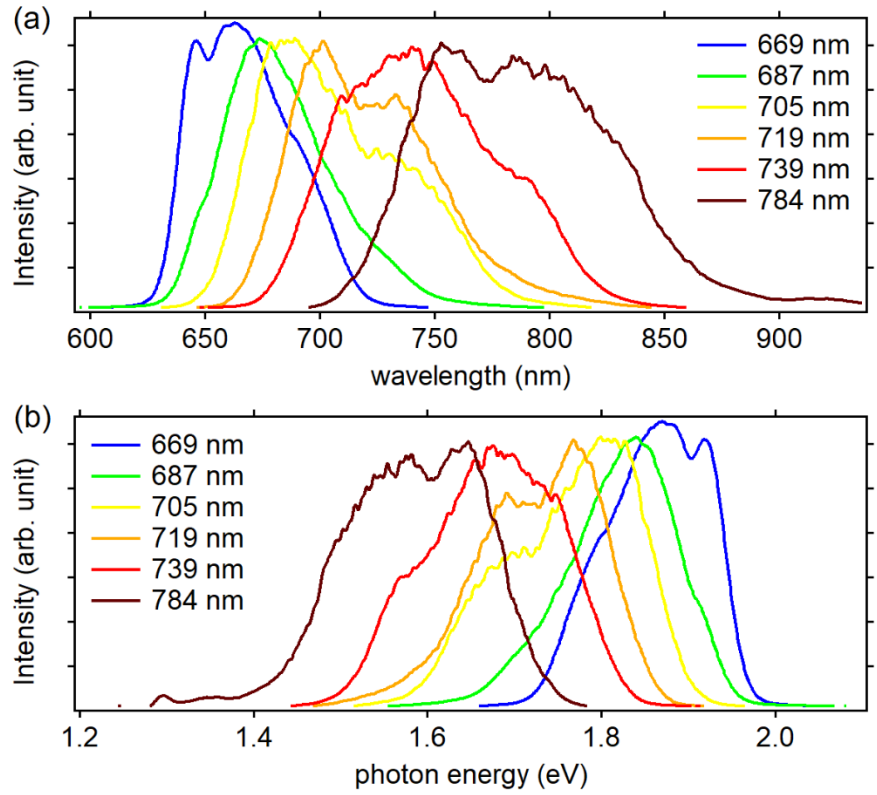

Figure S2: The spectra for the pump laser pulse used in the TR-TPPE experiment. The spectra are plotted as a function of (a) wavelength and (b) photon energy. The centroid wavelengths calculated with the spectra in (a) are shown in the figure ligand.